The Astrophysical Journal, 799:2 (11pp), 2015 January 20 doi:10.1088/0004-637X/799/1/2


# CORRELATIONS IN HORIZONTAL BRANCH OSCILLATIONS AND BREAK COMPONENTS IN XTE J1701-462 AND GX 17+2

Qing-cui Bu[1], Li Chen[1], Zhao-sheng Li[2], Jin-lu Qu[3], T. M. Belloni[4], and Liang Zhang[1]
[1] Department of Astronomy, Beijing Normal University, Beijing 100875, China; buqc@mail.bnu.edu.cn, chenli@bnu.edu.cn
[2] School of Physics and State Key Laboratory of Nuclear Physics and Technology, Peking University, Beijing 100871, China
[3] Laboratory for Particle Astrophysics, CAS, Beijing 100049, China; qujl@ihep.ac.cn
[4] INAF-Osservatorio Astronomico di Brera, Via E, Bianchi 46, I-23807 Merate (LC), Italy; tomaso.belloni@brera.inaf.it
*Received 2014 June 13; accepted 2014 November 4; published 2015 January 9*

## ABSTRACT

We studied the horizontal branch oscillations (HBO) and the band-limited components observed in the power spectra of the transient neutron star low-mass X-ray binary XTE J1701-462 and the persistent "Sco-like" Z source GX 17+2. These two components were studied based on the state-resolved spectra. We found that the frequencies of XTE J1701-462 lie on the known correlations (WK and PBK), showing consistency with other types of X-ray binaries (black holes, atoll sources, and millisecond X-ray pulsars). However, GX 17+2 is shifted from the WK correlation like other typical Z sources. We suggest that the WK/PBK main track forms a boundary that separates persistent sources from transient sources. The characteristic frequencies of break and HBO are independent of accretion rate in both sources, though it depends on spectral models. We also report the energy dependence of the HBO and break frequencies in XTE J1701-462 and how the temporal properties change with spectral state in XTE J1701-462 and GX 17+2. We studied the correlation between rms at the break and the HBO frequency. We suggest that HBO and break components for both sources probably arise from a similar physical mechanism: Comptonization emission from the corona. These two components could be caused by the same kind of oscillation in a corona with uneven density, and they could be generated from different areas of the corona. We further suggest that different proportions of the Comptonization component in the total flux cause the different distribution between GX 17+2 and XTE J1701-462 in the $\mathrm{rms_{break}}$–$\mathrm{rms_{HBO}}$ diagram.

*Key words:* accretion, accretion disks – black hole physics – stars: general – stars: neutron – X-rays: binaries – X-rays: stars

## 1. INTRODUCTION

Low-frequency quasi-periodic oscillations (LFQPOs) have been detected in most neutron star low-mass X-ray binaries (NS-LMXBs) and black hole low-mass X-ray binaries (BH-LMXBs; van der Klis 2006). Their centroid frequencies are typically ∼1–70 Hz for NS-LMXBs, while ∼0.01–30 Hz for BH-LMXBs. In LMXBs, the timing behavior has been shown to be strongly connected to the spectral properties (Hasinger & van der Klis 1989; van der Klis 1995, 2006; Homan et al. 2001; Belloni et al. 2004, 2005; Homan & Belloni 2005).

Based on X-ray spectra properties and rapid variability behaviors, bright NS-LMXBs are commonly classified into two sub-types, the Z sources and the atoll sources (Hasinger & van der Klis 1989). The Z sources have luminosities approaching the Eddington limit (∼0.1–1$L_{\mathrm{Edd}}$ or more), while the atoll sources show luminosities of ∼0.01–0.5$L_{\mathrm{Edd}}$. The color diagram (CD) and hardness intensity diagram (HID) of a typical Z source include three branches, the horizontal branch (HB), the normal branch (NB), and the flare branch (FB). Depending on further details about the shape and orientation of these branches, the Z sources were further classified into the "Cyg-like" Z sources and the "Sco-like" Z sources. Three distinct types of LFQPOs were observed in the Fourier power density spectra of Z sources: horizontal branch oscillation (HBO) with centroid frequency ∼9.5–60 Hz, normal branch oscillation (NBO) with centroid frequency ∼6–20 Hz, and flare branch oscillation (FBO) with centroid frequency ∼20 Hz. Atoll sources also show ∼20–60 Hz LFQPOs.

In the case of transient BH-LMXBs, LFQPOs have been sorted into type A, B, and C QPOs (see Wijnands et al. 1999b; Cui et al. 2000; Remillard et al. 2002; Casella et al. 2004; Zhang 2013; Motta et al. 2011). NS-LMXBs and BH-LMXBs have plenty of resemblances in their X-ray power spectra (Barret & Vedrenne 1995; Heindl & Smith 1998; Olive et al. 1998; Barret et al. 2000), particularly at high frequencies (van der Klis 1994a, 1994b; Berger & van der Klis 1998). Casella et al. (2005) suggested that the properties of type A, B, and C LFQPOs in BH-LMXBs are similar to those of FBOs, NBOs, and HBOs in Z sources, respectively. A universal correlation (known as the WK correlation) was found between the centroid frequencies of LFQPOs and break frequencies of band-limited components in BH-LMXBs, accreting millisecond pulsars, and atoll sources (Wijnands & van der Klis 1999a). Z sources also showed a tight correlation between HBO and break frequencies, only slightly shifted from the BH/atoll track. Psaltis et al (1999) found the PBK correlation, which links the lower kilohertz frequency quasi-periodic oscillations (kHz QPO) to LFQPOs in these systems. The LFQPOs involved in WK/PBK correlations in BH-LMXBs and NS-LMXBs were type C QPOs and HBOs, respectively. The WK and PBK correlations found in these different systems suggest that they were probably caused by a similar physical mechanism (Wagoner et al. 2001; Rezzolla et al. 2003).

The origin of LFQPOs in X-ray binaries has been discussed by several authors (Stella & Vietri 1998; Titarchuk & Osherovich 1999; Tagger & Pellat 1999; Done et al. 2007; Schnittman et al. 2006; Ingram et al. 2009). The Lense–Thirring (LT) precession mode, first introduced by Stella & Vietri (1998) to explain LFQPOs in NS-LMXB is deemed to be the most promising model in explaining LFQPOs. Despite their unclear origin, LFQPOs show a tight correlation with spectral states, which gives us an empirical way to study the accretion disk around compact objects. They could be key ingredients in understanding

**Table 1**
Data Selections for the Extraction of Hardness–Intensity Diagrams from XTE J1701-462 and GX 17+2

| Interval | Begin of Date (DD/MM/YY) | Begin of Obs. | End of Date (DD/MM/YY) | End of Obs. | Source Type |
|---|---|---|---|---|---|
| | | XTE J1701-462 | | | |
| A | 21/01/06 | 91106-01-04-00 | 31/01/06 | 91106-02-02-10 | Cyg-like |
| B | 02/02/06 | 91106-02-02-14 | 12/02/06 | 91442-01-01-02 | Cyg-like |
| C | 17/02/06 | 91442-01-07-02 | 26/02/06 | 91442-01-03-05 | Sco-like |
| D | 15/03/06 | 92405-01-02-05 | 23/03/06 | 92405-01-03-06 | Sco-like |
| | | GX 17+2 | | | |
| E | 03/10/99 | 40018-01-02-000 | 12/10/99 | 40018-01-01-18 | Sco-like |

the physical mechanism that modulates the different states. Meanwhile, the WK and PBK correlations suggested that LFQPOs probably have the same origin in these different systems, providing us with a new vision to study the physical mechanism of LFQPOs. Correlations between the PBK and WK have been widely studied in the BH and NS sources. The origin of LFQPOs in NS-LMXBs has been a controversial topic ever since they were discovered (Stella & Vietri 1998; Lin et al. 2012; Li et al. 2014; Altamirano et al. 2012; Homan 2012). The special shifted behavior of Z sources in the WK/PBK scheme made the physical mechanism of LFQPOs in NS-LMXBs somewhat more confusing.

XTE J1701-462 is a special transient NS-LMXB source that was discovered by the *RXTE* (Remillard & Lin 2006), which has gone through both types of Z behavior and, at the end of its outburst, became an atoll source (Homan et al. 2010). This source gives us a great opportunity to study the LFQPO mechanism among different subclasses of individual sources on the basis of the WK/PBK correlation. As a persistent "Sco-like" Z source, GX 17+2 displayed a roughly constant level over a long timescale, unlike XTE J1701-462, which was a transient (Wijnands et al. 1997; Homan et al. 2002). However, there is a strong similarity in spectral evolution between GX 17+2 and XTE J1701-462 (Lin et al. 2012; Li et al. 2014). Comparing these two sources could give us a contrasting view for studying the properties of HBOs and break components and investigating the shifted behavior of Z sources in WK/PBK correlations. In this paper, we present a detailed analysis of low-frequency power spectra of XTE J1701-462 and GX 17+2. Data reduction and analysis are described in Section 2. We give our results in Section 3. In Section 4, we discuss physical implications of our results, and a short summary is presented in Section 5.

## 2. DATA REDUCTION AND ANALYSIS

### 2.1. Data Selection

We analyzed all 866 observations of XTE J1701-462 obtained by the Proportional Counter Array (PCA) instrument on board *RXTE* during its 2006–2007 outburst. We chose 63 *RXTE* observations of GX 17+2 obtained in the period of 1999 October 3–12 (i.e., MJD 51454-51463) for a comparison study. For the reduction, we used the HEASOFT package, version 6.12. Only those data with elevation angles $>10^{\circ}$, pointing offsets $<0.01$, and South Atlantic Anomaly exclusion times of 30 minutes were selected for further analysis.

Type I X-ray bursts were identified and removed from the data. Background-subtracted light curves with 16 s time resolutions were constructed from the "standard 2" mode, using data from Proportional Counter Unit (PCU) number 2 only, without dead-time correction. For both XTE J1701-462 and GX 17+2, we defined two X-ray colors: a soft color (SC) and a hard color (HC), as the ratio of count rates in the ~4.5–7.4 keV/2.9–4.1 keV bands (PCA channels 10–17/6–9) and the ~10.2–18.1 keV/7.8–9.8 keV bands (PCA channels 24–43/18–23). Intensity was defined as the count rate in the energy range of ~2.9–18.1 keV(PCA channel 6–43). The small difference in the energy ranges caused by different epochs were ignored. The colors were used to produce CDs and HIDs. For XTE J1701-462, we divided the data into four time intervals, while all observations of GX 17+2 were combined as one interval. Data selections are listed in Table 1: for XTE J1701-462, intervals A and B correspond to the Cyg-like stage and intervals C and D to the Sco-like stage. Interval E is that from GX 17+2. The HIDs of all these five intervals are plotted in Figure 1.

### 2.2. Timing Analysis

Standard, fast Fourier transform (FFT) techniques (van der Klis 1989, 1995) were used to create power density spectra (PDS) from all active PCUs, adopting the rms normalization from Belloni & Hasinger (1990). The high time resolution single-bit and event mode data were used to create PDS, without background-subtraction or dead-time correction. We studied the properties of LFQPOs (in this case, HBOs) and band-limited components by selecting box regions along the HB in the HID, accumulating what are known as Sz-resolved spectra. The boxes for each interval are shown in Figure 1: each box corresponds to $>1600$ s of data. A rank number Sz was given for boxes to track their positions along the Z track (Hasinger et al. 1990). We set the Sz of the HB/NB vertex as one and the leftmost point of the HB as zero, also marked in Figure 1. The Sz of other boxes are obtained by spline interpolation (Dieters & van der Klis 2000; Lin et al. 2012; Li et al. 2014).

For each box, PDSs are accumulated from 16 s segments and a time bin of $2^{-8}$ s (yielding a frequency range of 0.0625–128 Hz), then averaged to obtain a single PDS per box. Since few photons are detected in very high energy bands, the channel range considered is 0–149, corresponding to energy range of 2–67 keV. We fitted the PDS with a multi-Lorentzian function (Nowak 2000; Belloni et al. 2002). PDSs were plotted as representations of rms$^2$ time frequencies ($\nu P_\nu$). It takes three to four Lorentzians to fit each PDS: the low-frequency noise (LFN, also as known as the band-limited component), the HBO and its second and third harmonics. Figure 2 shows a representative PDS of box 11 from interval A, with best-fit Lorentzians. Each Lorentzian, whether used to fit a QPO or band-limited noise, yields three parameters: a centroid frequency ($\nu_0$), a FWHM, and an integrated fractional rms. Then the characteristic

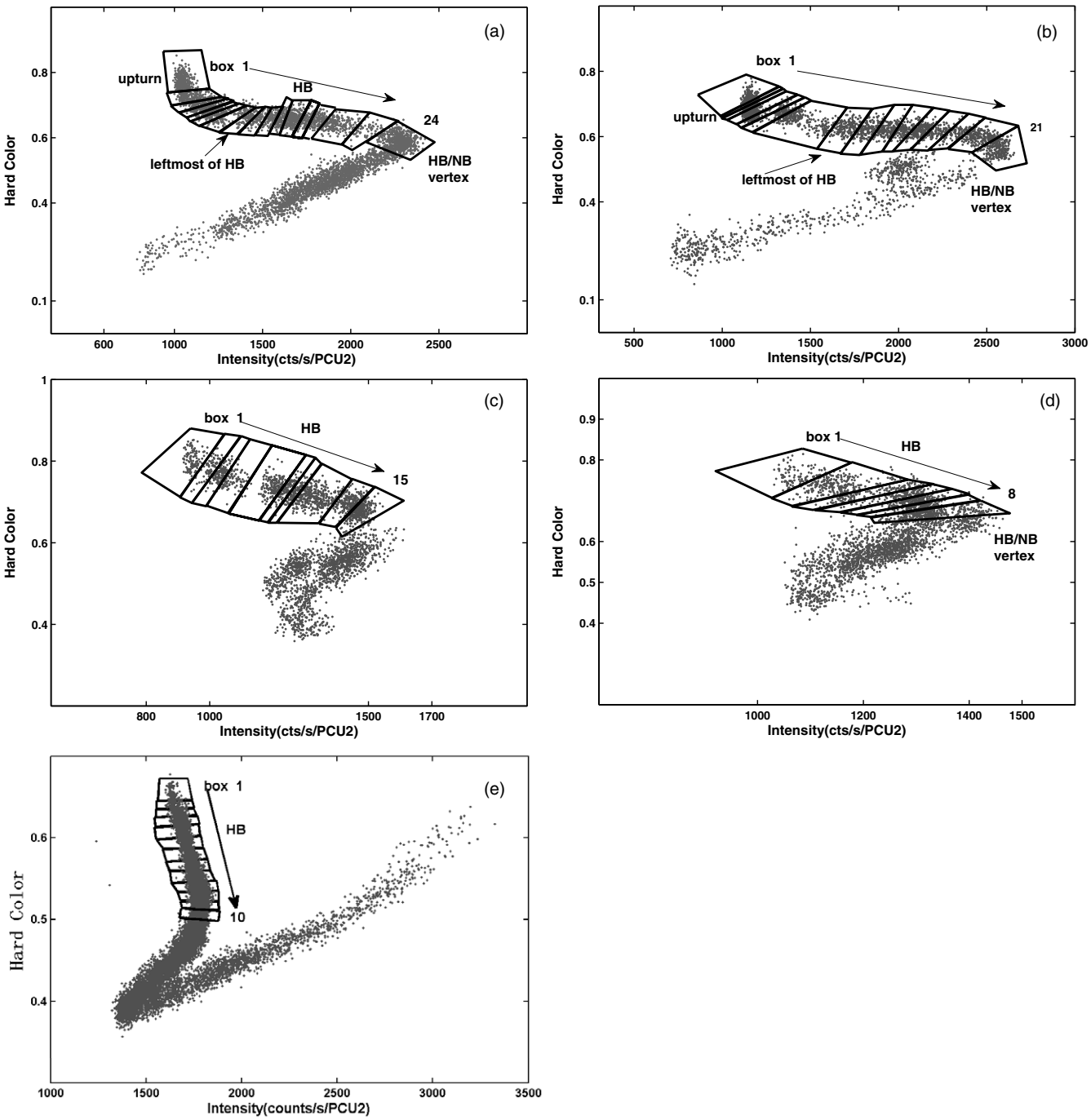


**Figure 1.** Hardness–intensity diagrams and box division of the five intervals listed in Table 1, with their interval numbers indicated in each panel. Panels (a)–(d) are extracted from XTE J1701-462 and panel (e) is extracted from GX 17+2. Each dot represents 16 s of background-subtracted data from PCU 2. See more details in the text.

frequency $\nu_c$ for a particular component can be calculated by using $\nu_c = \sqrt{\nu_0^2 + (\mathrm{FWHM}/2)^2}$, as introduced by Belloni et al. (2002). We will indicate the characteristic frequency of the HBO as $\nu_{\mathrm{HBO}}$ and that of the band-limited component as $\nu_{\mathrm{break}}$.

In order to study the energy dependence of the HBO and band-limited components, we further divided the PCA channel 0–149 interval into six sub-channels. The division of energy channels and their corresponding centroid energies are listed in Table 2. The multi-Lorentzian fitting results for all selected boxes are listed in Table 3.

**Table 2**
*RXTE*/PCA Energy Bands for XTE J1701-462 Used in This Work

| PCA Channel | Energy Band (keV) | Centroid Energy (keV) |
|---|---|---|
| 0–10 | 2–4.5 | 3.25 |
| 11–13 | 4.5–5.7 | 5.1 |
| 14–16 | 5.7–6.9 | 6.3 |
| 17–22 | 6.9–9.4 | 8.2 |
| 23–35 | 9.4–14.8 | 12.1 |
| 36–149 | 14.8–65 | 16.5 |

**Table 3**
Results from a Multi-Lorentzian Fitting for Each Box in Figure 1

| Box Number | Sz | $\nu_{\rm break}$ (Hz) | $\rm rms_{break}$ (%) | $\nu_{\rm HBO}$ (Hz) | $\rm rms_{HBO}$ (%) |
|---|---|---|---|---|---|
| | | XTE J1701-462 Cyg-like interval A | | | |
| 1 | −0.30 | 2.8 ± 0.1 | 19.3 ± 3.2 | 12.1 ± 0.1 | 8.6 ± 0.5 |
| 4 | −0.19 | 3.5 ± 0.1 | 14.3 ± 1.0 | 22.9 ± 0.4 | 7.5 ± 0.6 |
| 5 | −0.17 | 4.0 ± 0.0 | 16.3 ± 1.8 | 24.7 ± 0.3 | 6.6 ± 0.5 |
| 6 | −0.13 | 4.3 ± 0.0 | 17.1 ± 2.2 | 26.8 ± 0.3 | 6.0 ± 0.5 |
| 7 | −0.08 | 4.6 ± 0.2 | 14.7 ± 1.6 | 28.4 ± 0.3 | 6.0 ± 0.5 |
| 8 | 0 | 6.3 ± 0.5 | 10.3 ± 0.6 | 31.7 ± 0.5 | 5.6 ± 0.5 |
| 9 | 0.07 | 6.6 ± 0.4 | 11.9 ± 0.6 | 35.3 ± 0.2 | 4.4 ± 0.4 |
| 10 | 0.15 | 6.9 ± 1.1 | 12.2 ± 3.2 | 37.0 ± 0.3 | 4.1 ± 0.4 |
| 11 | 0.21 | 6.9 ± 0.6 | 11.6 ± 1.6 | 39.3 ± 0.4 | 4.0 ± 0.4 |
| 12 | 0.33 | 7.7 ± 0.7 | 11.1 ± 0.5 | 41.0 ± 0.5 | 3.4 ± 0.4 |
| 13 | 0.40 | 7.3 ± 0.3 | 13.5 ± 0.7 | 41.9 ± 0.6 | 3.2 ± 0.4 |
| 14 | 0.49 | 9.9 ± 0.9 | 8.9 ± 0.6 | 43.2 ± 1.0 | 2.9 ± 0.5 |
| 15 | 0.60 | 9.2 ± 0.2 | 13.0 ± 0.7 | 46.8 ± 1.2 | 2.1 ± 0.5 |
| 16 | 0.81 | 12.1 ± 1.6 | 6.1 ± 0.6 | 48.7 ± 1.2 | 2.2 ± 0.6 |
| 17 | 1 | 8.6 ± 0.6 | 3.5 ± 0.2 | 51.6 ± 0.7 | 1.7 ± 0.2 |
| | | XTE J1701-462 Cyg-like interval B | | | |
| 1 | −0.40 | 2.2 ± 0.0 | 15.9 ± 1.4 | 13.0 ± 0.2 | 8.8 ± 0.5 |
| 2 | −0.38 | 2.5 ± 0.0 | 16.6 ± 1.6 | 14.3 ± 0.2 | 8.6 ± 0.5 |
| 3 | −0.38 | 2.5 ± 0.0 | 16.2 ± 1.4 | 14.9 ± 0.2 | 8.5 ± 0.4 |
| 4 | −0.37 | 2.9 ± 0.1 | 18.0 ± 2.5 | 15.4 ± 0.1 | 7.7 ± 0.5 |
| 5 | −0.34 | 3.3 ± 0.2 | 17.2 ± 3.2 | 16.7 ± 0.2 | 6.7 ± 0.6 |
| 6 | −0.20 | 4.5 ± 0.1 | 19.2 ± 4.4 | 33.0 ± 0.3 | 4.4 ± 0.5 |
| 7 | −0.07 | 5.6 ± 0.3 | 13.9 ± 0.8 | 34.2 ± 0.2 | 4.6 ± 0.4 |
| 8 | 0.16 | 6.6 ± 0.4 | 12.2 ± 0.5 | 37.1 ± 0.3 | 4.2 ± 0.3 |
| 9 | 0.28 | 6.8 ± 0.5 | 12.9 ± 1.7 | 39.1 ± 0.5 | 3.9 ± 0.4 |
| 10 | 0.38 | 7.7 ± 0.4 | 11.9 ± 0.5 | 41.2 ± 0.6 | 3.8 ± 0.4 |
| 11 | 0.48 | 8.7 ± 0.6 | 10.5 ± 0.5 | 42.1 ± 1.2 | 3.2 ± 0.5 |
| 12 | 0.58 | 10.0 ± 0.8 | 8.8 ± 0.5 | 43.1 ± 1.3 | 3.2 ± 0.5 |
| 13 | 0.68 | 11.1 ± 1.4 | 8.2 ± 1.1 | 44.4 ± 1.2 | 2.8 ± 0.5 |
| 14 | 0.77 | 11.4 ± 1.0 | 7.7 ± 0.5 | 45.2 ± 1.1 | 2.7 ± 0.5 |
| 16 | 0.91 | 11.5 ± 0.5 | 10.2 ± 0.9 | 48.2 ± 2.1 | 2.4 ± 0.6 |
| 17 | 1 | 10.2 ± 1.1 | 4.2 ± 0.3 | 51.3 ± 0.9 | 2.0 ± 0.3 |
| | | XTE J1701-462 Sco-like interval C | | | |
| 1 | 0 | 6.0 ± 0.1 | 15.5 ± 1.5 | 27.9 ± 0.2 | 5.6 ± 0.4 |
| 2 | 0.09 | 6.2 ± 0.04 | 14.5 ± 1.7 | 32.3 ± 0.3 | 4.6 ± 0.5 |
| 3 | 0.15 | 6.4 ± 0.1 | 14.9 ± 2.1 | 34.2 ± 0.3 | 4.0 ± 0.5 |
| 4 | 0.26 | 6.6 ± 0.1 | 14.2 ± 2.0 | 35.9 ± 0.4 | 3.3 ± 0.5 |
| 5 | 0.46 | 8.8 ± 0.6 | 10.2 ± 0.9 | 43.6 ± 0.8 | 1.5 ± 2.5 |
| 6 | 0.53 | 8.9 ± 1.3 | 7.9 ± 1.3 | 45.0 ± 1.1 | 1.5 ± 0.7 |
| 7 | 0.59 | 9.6 ± 1.3 | 6.9 ± 0.6 | 46.5 ± 1.6 | 1.6 ± 0.8 |
| 8 | 0.70 | 9.8 ± 0.6 | 8.4 ± 0.6 | 48.9 ± 1.3 | 1.3 ± 0.6 |
| 9 | 0.88 | 9.7 ± 0.5 | 7.7 ± 0.8 | 53.3 ± 1.6 | 1.4 ± 0.6 |
| 10 | 0.98 | 11.1 ± 0.5 | 9.3 ± 1.3 | 56.8 ± 2.5 | 2.8 ± 1.0 |
| | | XTE J1701-462 Sco-like interval D | | | |
| 1 | 0 | 8.7 ± 0.7 | 8.7 ± 0.6 | 43.2 ± 1.0 | 2.1 ± 0.5 |
| 2 | 0.32 | 10.2 ± 0.4 | 9.2 ± 0.8 | 47.1 ± 1.5 | 1.1 ± 0.7 |
| 3 | 0.56 | 9.6 ± 1.1 | 6.7 ± 0.5 | 46.2 ± 1.2 | 1.3 ± 0.6 |
| 4 | 0.78 | 10.1 ± 1.7 | 6.2 ± 1.0 | 52.9 ± 1.4 | 1.5 ± 0.5 |
| 5 | 0.89 | 8.7 ± 0.3 | 8.6 ± 1.1 | 56.6 ± 3.4 | 2.2 ± 1.0 |
| 6 | 0.95 | 8.7 ± 1.5 | 3.3 ± 0.4 | 58.2 ± 1.8 | 1.3 ± 0.6 |
| 7 | 1 | 9.7 ± 1.7 | 4.1 ± 0.5 | 60.7 ± 1.6 | 1.9 ± 0.6 |
| | | GX 17+2 interval E | | | |
| 1 | 0.01 | 2.4 ± 0.5 | 6.2 ± 1.0 | 23.3 ± 0.7 | 3.1 ± 0.5 |
| 2 | 0.06 | 2.7 ± 0.3 | 6.0 ± 0.6 | 26.3 ± 0.5 | 3.0 ± 0.5 |
| 3 | 0.09 | 2.8 ± 0.4 | 6.1 ± 0.6 | 27.4 ± 0.4 | 2.9 ± 0.4 |
| 4 | 0.10 | 3.2 ± 0.3 | 6.5 ± 0.4 | 28.5 ± 0.3 | 2.8 ± 0.3 |
| 5 | 0.21 | 3.0 ± 0.4 | 5.8 ± 0.6 | 29.4 ± 0.4 | 2.4 ± 0.4 |
| 6 | 0.40 | 4.1 ± 0.5 | 6.4 ± 0.4 | 35.3 ± 1.1 | 2.0 ± 0.5 |
| 7 | 0.52 | 4.2 ± 0.2 | 5.7 ± 0.2 | 37.8 ± 0.5 | 1.7 ± 0.3 |
| 8 | 0.68 | 4.5 ± 0.2 | 5.5 ± 0.2 | 39.3 ± 0.6 | 1.5 ± 0.2 |
| 9 | 0.78 | 5.0 ± 0.3 | 5.2 ± 0.2 | 42.0 ± 0.4 | 1.0 ± 0.2 |
| 10 | 0.91 | 5.4 ± 0.3 | 4.9 ± 0.2 | 44.2 ± 0.6 | 0.9 ± 0.2 |

**Note.** The parameters of both band-limited and HBO components are shown here.

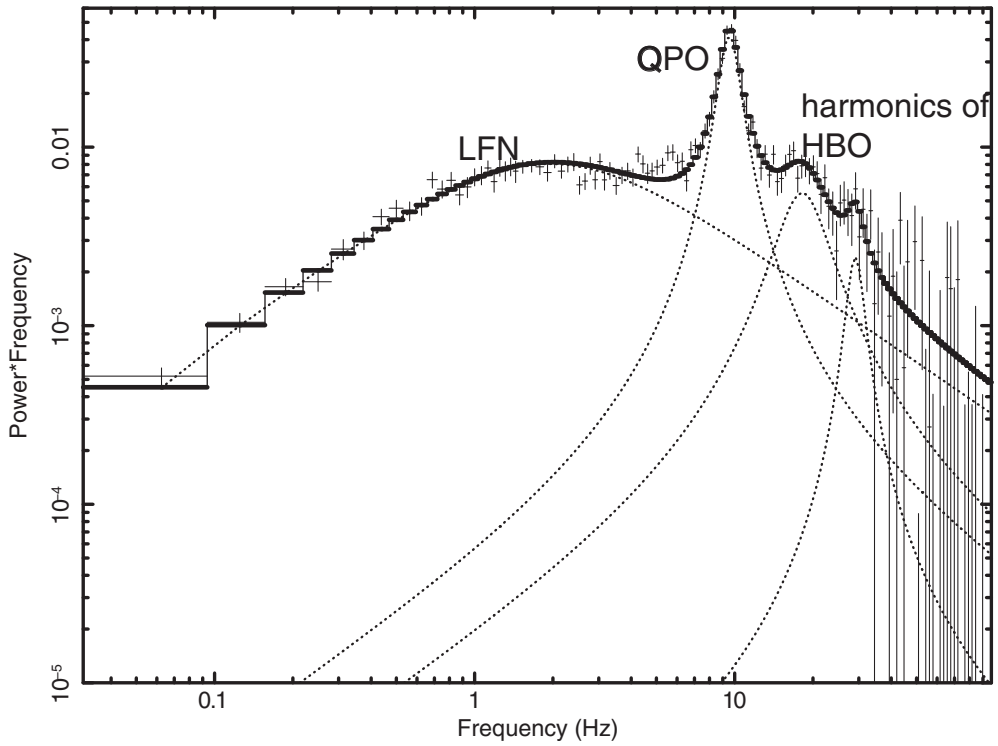


**Figure 2.** Typical power density spectrum of box 11 in interval A of XTE J1701-462 together with the different best-fit Lorentzian components.

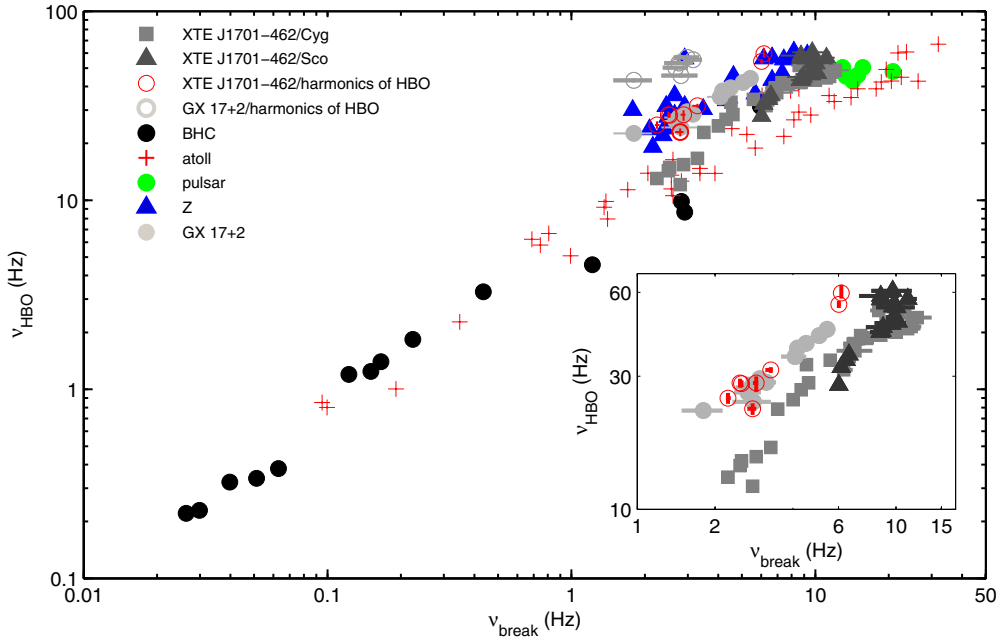


**Figure 3.** WK correlation involved with XTE J1701-462 and GX 17+2. The inset panel at the lower right shows a zoomed-in version of our data with error bars.

## 3. RESULTS

### *3.1. The WK Correlation of XTE J1701-462 and GX 17+2*

In the PDS corresponding to different boxes, for XTE J1701-462, we found $\nu_{HBO}$ between ∼10 Hz and ∼60 Hz. These HBOs are all accompanied by $\nu_{break}$ between ∼2 Hz and ∼12 Hz. For GX 17+2, $\nu_{HBO}$ between ∼22 Hz and ∼45 Hz are found, with $\nu_{break}$ between ∼2 Hz and ∼5 Hz. We also consider data from Wijnands & van der Klis (1999a) and Altamirano et al. (2012). The corresponding WK correlation is shown in Figure 3. Our points from XTE J1701-462 lie on the main WK track, between the outer edge of atoll sources and the lower edge of Z sources, covering most of the points from the 11 Hz accreting pulsar IGR J17480-2446. Meanwhile, the points from the Sco-like stage, with frequency ranges of ∼30–60 Hz, are blanketed with the points from the Cyg-like stage. It is worth noticing that, based on the data of XTE J1701-462, BHCs and part of the atoll sources are on a straight line. However, our data points for GX 17+2 are distributed in the upper envelop of XTE J1701-462, overlapping the data of typical Z sources, showing a slightly

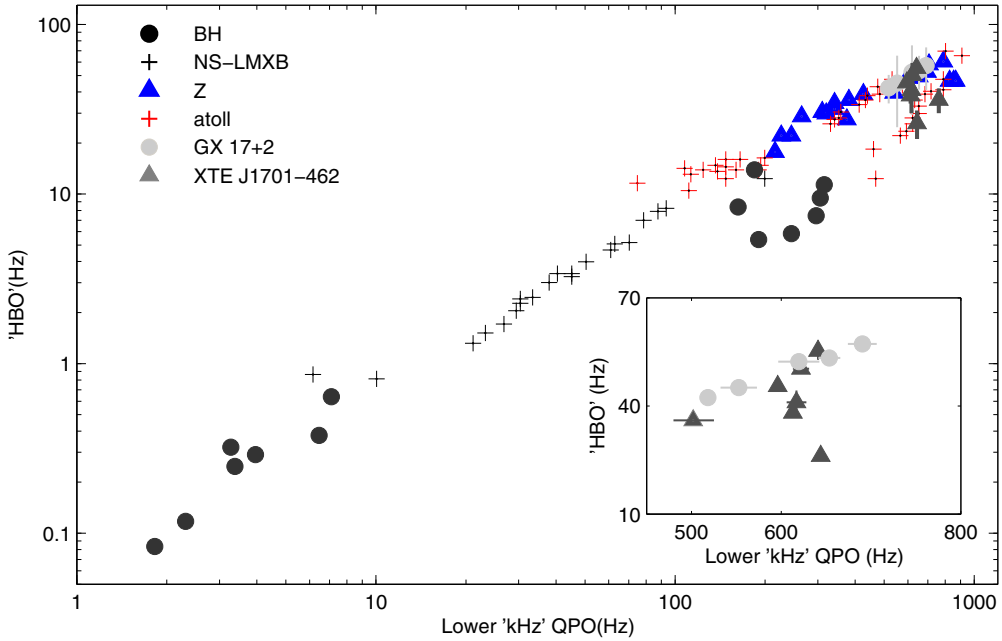


**Figure 4.** PBK relation, including XTE J1701-462 and GX 17+2. The inset panel at the lower right shows a zoomed-in version of our data with error bars.

shifted correlation from the main cone. It is worth emphasizing that part of the Z data taken from the literature also belonged to GX 17+2, extracted from earlier observation. Our result for the WK correlation is consistent with what Wijnands & van der Klis (1999a) had found in GX 17+2.

### 3.2. The Shifted Behavior of Z Sources in the WK Correlation

To study the shifted behavior of Z sources, we further plotted the second harmonic frequencies of HBOs ($\nu_2$) for both sources in the WK correlation. We found that the points of $\nu_2$ from XTE J1701-462 overlap with the points of $\nu_{\rm HBO}$ from GX 17+2 and typical Z sources. Furthermore, the points of $\nu_2$ from GX 17+2 are distributed on the upper side of typical Z sources.

### 3.3. The PBK Correlation of XTE J1701-462 and GX 17+2

We then tested our identification using the PBK relation using the lower kHz QPO frequency ($\nu_{\rm low}$) and $\nu_{\rm HBO}$. We didn't measure the kHz QPO frequencies ourselves. Since Sanna et al. (2010) already found 14 observations with kHz QPO in XTE J1701-462, we further searched the HBO signal in these observations to study the PBK relation. Seven observations are found with both $\nu_{\rm low}$ and $\nu_{\rm HBO}$ in the Sco-like stage, with their IDs and frequencies listed in Table 4. In this case, we only accumulated one PDS per observation in order to directly use the results from Sanna et al. (2010). For GX 17+2, Lin et al. (2012) had measured the kHz QPOs and HBOs on Sz-resolved spectra. Since we chose the same data segment with Lin et al. (2012), we simply used their data, which are also listed in Table 4. In Figure 4, we plot the PBK correlation using the data from Table 4 together with the data from Psaltis et al (1999). The data of GX 17+2 are on the main relation, showing good consistency with atoll sources and part of BHCs. However, as can be seen in the inset of Figure 4, the data of XTE J1701-462 show a larger spread around the correlation than those of GX 17+2, overlapping with the data of GX 17+2 and atoll sources (4U 1608–52 and 4U 1728–34).

**Table 4**
Data We Used to Study the PBK Correlation in XTE J1701-462 and GX 17+2

| Observation[a] (Sz) | $\nu_{\rm HBO}$ (Hz) | $\nu_{\rm low}$ (Hz) |
|---|---|---|
| XTE J1701-462 | | |
| 91442-01-07-09 | $55.3 \pm 2.5$ | $642.7 \pm 3.1$ |
| 92405-01-01-02 | $38.1 \pm 0.4$ | $615.1 \pm 3.8$ |
| 92405-01-01-04 | $36.0 \pm 0.4$ | $502.4 \pm 23.1$ |
| 92405-01-02-03 | $50.3 \pm 1.3$ | $623.9 \pm 8.3$ |
| 92405-01-02-05 | $45.5 \pm 0.8$ | $595.9 \pm 10.1$ |
| 92405-01-03-05 | $41.0 \pm 3.3$ | $612.5 \pm 7.7$ |
| 92405-01-40-04 | $26.1 \pm 0.2$ | $650.5 \pm 7.1$ |
| GX 17+2 | | |
| 0.80–0.88 | $42.3 \pm 0.5$ | $518.2 \pm 6$ |
| 0.88–0.96 | $45.1 \pm 0.7$ | $552.6 \pm 20.3$ |
| 1.00–1.04 | $52.3 \pm 0.9$ | $619.5 \pm 22.9$ |
| 1.04–1.12 | $53.3 \pm 1.7$ | $653.6 \pm 12.2$ |
| 1.12–1.20 | $57.2 \pm 0.9$ | $690.3 \pm 16.1$ |

**Notes.** [a] The data we used in this table are all extracted from Sanna et al. (2010) and Lin et al. (2012). ObsID and Sz were used separately in their work.

### 3.4. The Energy Dependence of HBO and Band-limited Components in XTE J1701-462

In order to test the hypothesis that the band-limited and HBO components have the same origin, we analyzed the data from the six sub-channels (listed in Table 2, see above). In XTE J1701-462, seven boxes (with six of them in the Cyg-like stage and one in the Sco-like stage) were selected from four intervals, judging by the appearance of HBO signals in all six sub-channels. We also investigated the energy dependence of the rms amplitude of the components ($\rm rms_{break}$ and $\rm rms_{HBO}$). When calculating the rms amplitude, we took into account the background contribution to convert power to rms amplitude. We neglected the background contribution for the total energy band since its effect is negligible, but considered its contribution for all the

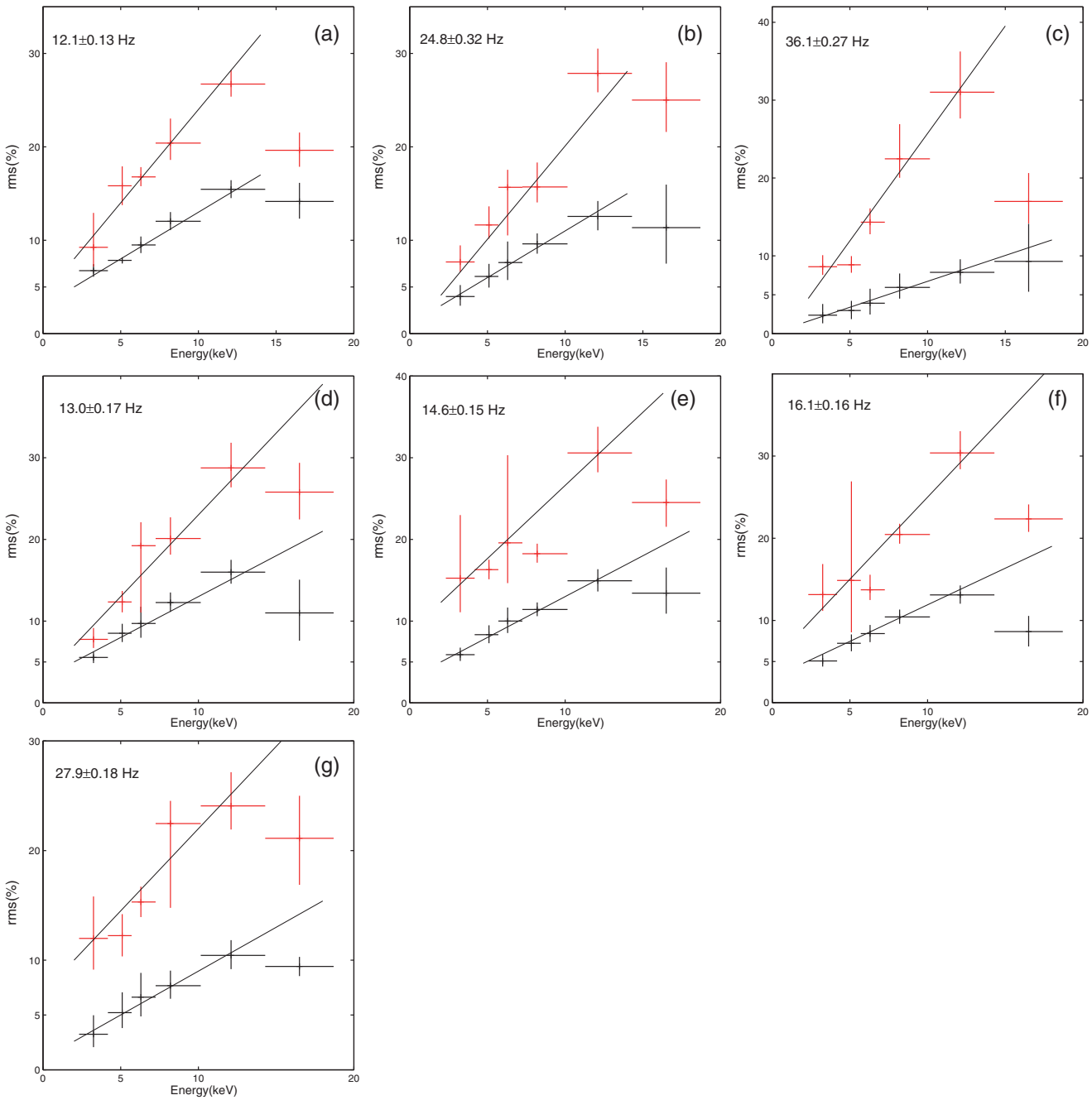


**Figure 5.** This figure shows the rms–energy relation for seven selected boxes. Panels (a)–(e) are extracted from the Cyg-like stage while panel (g) is extracted from the Sco-like stage of XTE J1701-462. The horizontal branch oscillation frequencies are marked in the upper left part of each sub-figure. Red crosses and black crosses represent $\mathrm{rms_{break}}$ and $\mathrm{rms_{HBO}}$, respectively.

sub-channel bands. The formula is $\mathrm{rms} = \sqrt{(P/S+B)} * (S + B/S)$, where S and B stand for source and background count rates, and P is the power normalized according to Leahy. We also considered the systematic uncertainty into the background as introduced by Jahoda et al. (2006). Figure 5 shows the rms–energy correlation for these two components. The values of $\nu_{\mathrm{HBO}}$ are indicated in the upper left corner of each sub-figure. The trends of $\mathrm{rms_{break}}$ and $\mathrm{rms_{HBO}}$ with energy are similar in both Cyg-like and Sco-like stages. Both $\mathrm{rms_{break}}$ and $\mathrm{rms_{HBO}}$ increase significantly with photon energy below ∼12 keV, and stay more or less constant after ∼12 keV. We used straight lines to fit the first five data points for both components, respectively. The fitting results are listed in Table 5, with errors given at $1\sigma$ level. R-squared represents the coefficient of determination, indicating how well the model fits the data. We found that the slopes for the break component (a1) are consistent with each other within the error (∼0.2) in all seven sub-figures, while those for the HBO component (a2) also have the same value (∼0.1) within the error. However, for GX 17+2, the detection significance of HBOs in six energy bands are not good enough to do the similar work as in XTE J1701-462. We could not give a comparative result in GX 17+2.

### *3.5. The Sz Dependence of HBO and Band-limited Components in XTE J1701-462 and GX 17+2*

In Figure 6, we plot $\mathrm{rms_{break}}$ and $\mathrm{rms_{HBO}}$ as a function of Sz for all five intervals, to study how the temporal properties change with the different positions in the HID. Our results show that

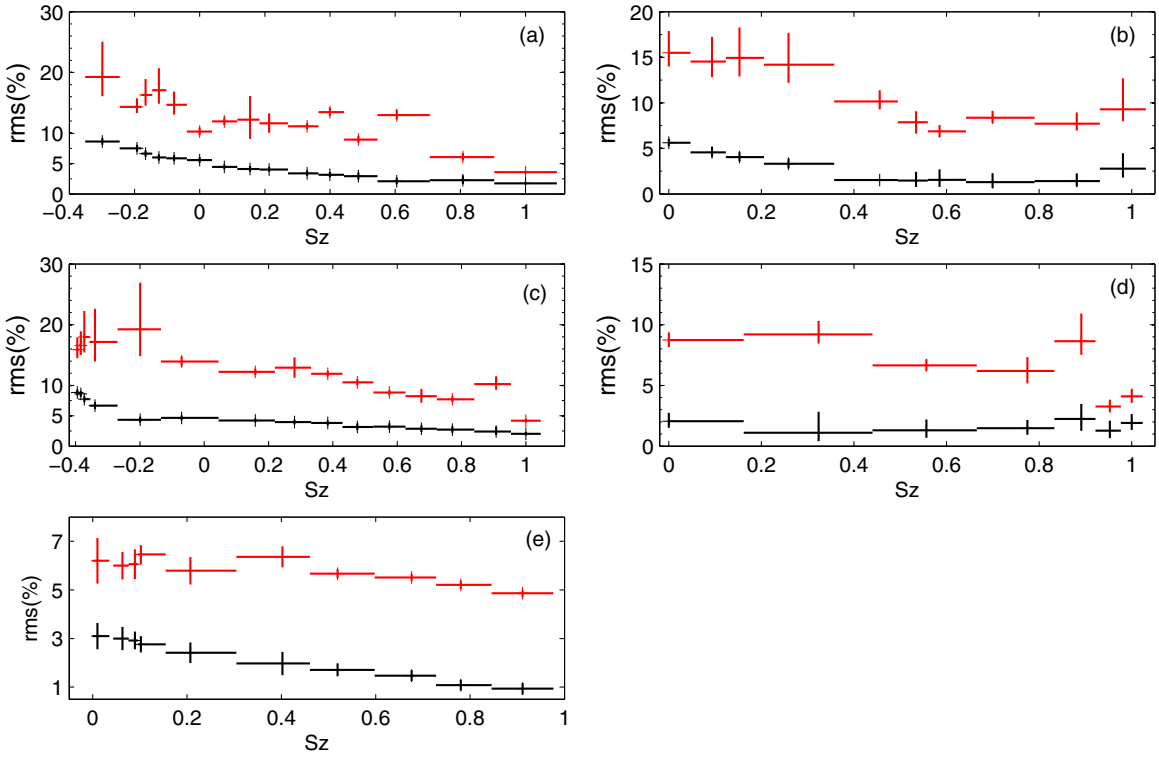


**Figure 6.** rms–Sz relation of XTE J1701-462 and GX 17+2. Panels (a)–(d) correspond, respectively, to intervals A–D, while panel (e) corresponds to interval E. Each subfigure shows the values of rms evolving from the (leftmost HB) upturn HB to the HB/NB vertex. Red crosses and black crosses represent $\mathrm{rms_{break}}$ and $\mathrm{rms_{HBO}}$, respectively.

**Table 5**
The Parameters Used to Fit the rms–Energy Correlation of Two Components in Figure 5

| Figure Number | break | | | HBO | | |
|---|---|---|---|---|---|---|
| | a1 | b1 | R1-squared | a2 | b2 | R2-squared |
| a | $0.02 \pm 0.003$ | $0.04 \pm 0.02$ | 0.97 | $0.01 \pm 0.001$ | $0.03 \pm 0.001$ | 0.99 |
| b | $0.02 \pm 0.003$ | $0.001 \pm 0.03$ | 0.95 | $0.01 \pm 0.001$ | $0.01 \pm 0.006$ | 0.99 |
| c | $0.03 \pm 0.004$ | $-0.01 \pm 0.03$ | 0.97 | $0.01 \pm 0.001$ | $0.00 \pm 0.006$ | 0.97 |
| d | $0.02 \pm 0.004$ | $0.03 \pm 0.03$ | 0.94 | $0.01 \pm 0.001$ | $0.03 \pm 0.001$ | 0.99 |
| e | $0.02 \pm 0.003$ | $0.09 \pm 0.02$ | 0.93 | $0.01 \pm 0.001$ | $0.03 \pm 0.007$ | 0.98 |
| f | $0.02 \pm 0.004$ | $0.05 \pm 0.02$ | 0.93 | $0.01 \pm 0.001$ | $0.03 \pm 0.006$ | 0.99 |
| g | $0.015 \pm 0.004$ | $0.07 \pm 0.03$ | 0.90 | $0.01 \pm 0.001$ | $0.01 \pm 0.006$ | 0.98 |

**Note.** The parameters with $1\sigma$ errors are given in the table; R-squared stands for the coefficient of determination.

both $\mathrm{rms_{HBO}}$ and $\mathrm{rms_{break}}$ show similar trends in all five intervals, i.e., they all decrease with Sz. However, the rms values change more obviously in Cyg-like intervals than in Sco-like intervals. For instance, $\mathrm{rms_{break}}$ (red crosses) decline from 19% to 4% in both Cyg-like intervals. $\mathrm{rms_{break}}$ changes less in Sco-like intervals, decreasing from 16% to 8% in Sco-like interval C and dropping from 9% to 4% in Sco-like interval D. The values of $\mathrm{rms_{HBO}}$ decline from 9% to 2% in two Cyg-like intervals, while they drop from 6% to 1% in Sco-like interval C. The values of $\mathrm{rms_{HBO}}$ and $\mathrm{rms_{break}}$ in GX 17+2 are close to those of Sco-like interval D in XTE J1701-462, that is, $\mathrm{rms_{HBO}}$ decreases from $\sim$3% to 1% and $\mathrm{rms_{break}}$ decreases from $\sim$6% to 5%.

### *3.6. The $\mathrm{rms_{break}}$–$\mathrm{rms_{HBO}}$ Correlation in XTE J1701-462 and GX 17+2*

To further investigate the correlations between HBO and break components in XTE J1701-462 and GX 17+2, we plot the relation between $\mathrm{rms_{break}}$ and $\mathrm{rms_{HBO}}$ in Figure 7(a). It is interesting to notice that the points of the HB/NB vertex from XTE J1701-462 are distributed separately from those of the HB, with the points of GX 17+2 lying between them. To make the correlation more clear, we further rebinned the adjacent points in terms of $\Delta\mathrm{rms_{HBO}} < 0.5$ to reduce errors, and plot the result in Figure 7(b). We did not rebin the data of the HB/NB vertex because there are only four of them. We used a power law to fit the data of GX 17+2 and J1701-462 separately (excluding the data of HB/NB vertex because of its different physical origin from HB (Lin et al. 2012)). We obtained $\mathrm{rms_{break}} = (6.69 \pm 1.17) * \mathrm{rms_{HBO}}^{(0.46\pm0.04)}$ for XTE J1701-462 and $\mathrm{rms_{break}} = (5.18 \pm 0.51) * \mathrm{rms_{HBO}}^{(0.17\pm0.09)}$ for GX 17+2, with $1\sigma$ errors. The difference between the two power-law indices is different from zero at a 99.5% confidence level ($2.8\sigma$).

## 4. DISCUSSION

We studied the HBOs and band-limited components observed in the transient NS-LMXB XTE J1701-462 and the persistent "Sco-like" Z source GX 17+2. Figure 3 shows that the data

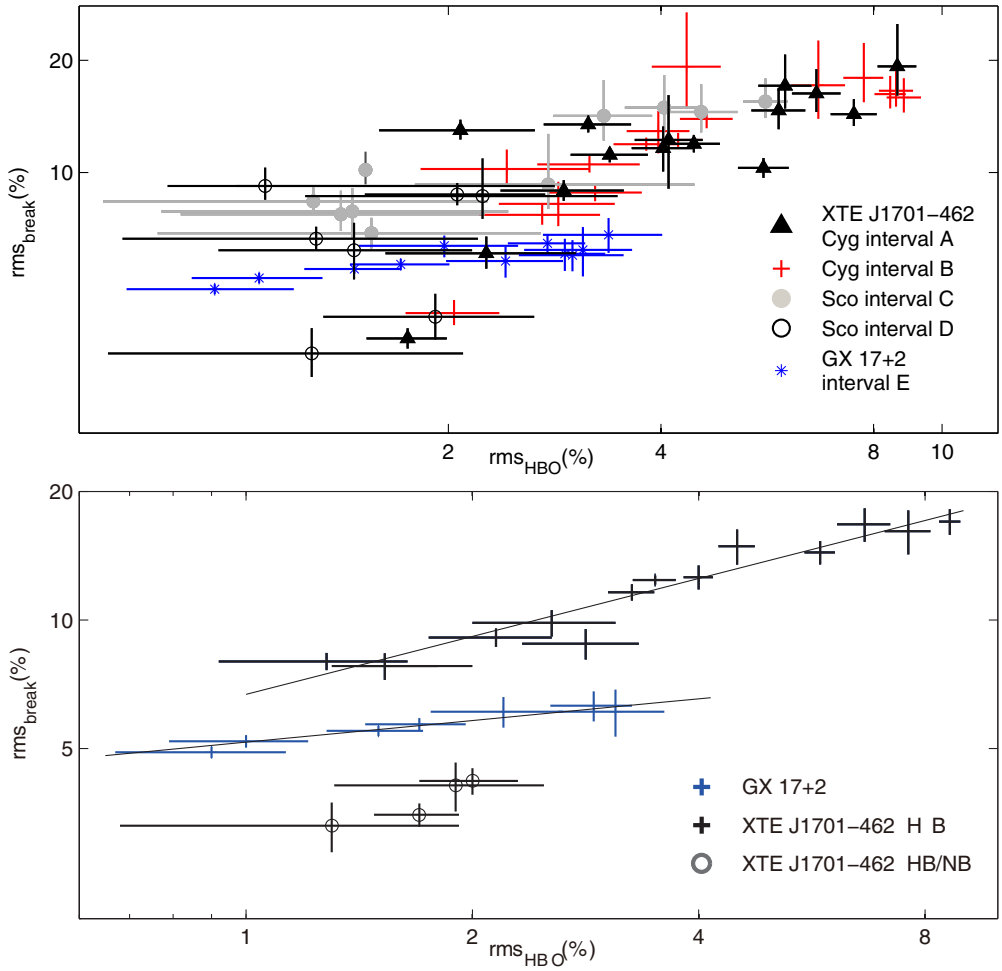


**Figure 7.** $rms_{break}$–$rms_{HBO}$ relation for XTE J1701-462 and GX 17+2. Figure 7(b) is a rebinned version of Figure 7(a). The data in ellipse are extracted from HB/NB vertexes of XTE J1701-462.

points of XTE J1701-462 are on the main relation of WK schema, lying between atoll sources and the typical persistent Z sources (Cyg X-2, GX 5–1, GX 340+0, Sco X-1), without a significant shift. The data points of GX 17+2 are shifted from the main correlation, overlapping with data of the typical persistent Z sources extracted from Wijnands & van der Klis (1999a). In addition, the data points of the second harmonics of the HBO from XTE J1701-462 overlap with the data of fundamental HBO frequency from GX 17+2. Figure 4 shows that GX 17+2 is on the main PBK correlation, covering the data of typical persistent Z sources, while XTE J1701-462 lies between typical persistent Z sources and atoll sources. Both $rms_{break}$ and $rms_{HBO}$ increase with photon energy below ~12 keV and drop above ~12 keV in XTE J1701-462. Furthermore, both $rms_{break}$ and $rms_{HBO}$ decrease along HB in XTE J1701-462 and GX 17+2. We also found that $rms_{break}$ increases as a power law with $rms_{HBO}$ for both sources, only with different rates of increase.

### *4.1. WK/PBK Implication in XTE J1701-462 and GX 17+2*

XTE J1701-462 is on the main track of the WK relation, together with BHCs, atoll sources, while GX 17+2 is shifted from the main track like other persistent Z sources (Cyg X-2, GX 5–1, GX 340+0, Sco X-1, and an earlier observation of GX 17+2). Wijnands & van der Klis (1999a) suggested that the HBOs observed in shifted Z sources are probably harmonic frequencies. However, according to our results, the HBOs in GX 17+2 and XTE J1701-462 should be the same type of QPO since they have similar frequency and rms values. GX 17+2 is a persistent Sco-like Z source that shows strong similarities in spectral properties with XTE J1701-462 in its Sco-like stage (Lin et al. 2012; Li et al. 2014). In Figure 5, one can also see that the $rms_{HBO}$ of both GX 17+2 and XTE J1701-462 decreases along the HB, while the values of $rms_{HBO}$ in GX 17+2 are close to those of the Sco-like interval D in XTE J1701-462. All of these results suggest the HBOs in GX 17+2 have similar properties with those in XTE J1701-462, or even in other types of sources. The HBOs in GX 17+2 should also be fundamental QPOs, not harmonics. Thus, the shifted Z track in WK correlation should be caused by HBOs in persistent Z sources, not harmonics, even the harmonics of HBOs in XTE J1701-462 overlap with the shifted Z track.

XTE J1701-462 has a more scattered distribution than GX 17+2 in the PBK correlation. This could be caused by the existence of two different types of lower kHz QPOs (Psaltis et al. 1999). GX 17+2 is a persistent Z source whose temporal and spectral properties barely change with time, which could explain the consistency with other typical persistent Z sources (Cyg X-2, GX 5–1, GX 340+0, and Sco X-1) in the WK and PBK correlations. XTE J1701-462 and GX 17+2 are both Z sources and exhibit strong similarities in spectral and fast

variability properties (Lin et al. 2012; Li et al. 2014). However, they lie on different tracks in the WK and PBK correlations, which makes the physical mechanism behind these correlations more mysterious.

The WK and PBK correlations between these X-ray sources show that the solid surface, the magnetosphere, and absorption along the line of sight do not affect these rapid variability components (Wijnands & van der Klis 1999a). These similarities suggested that the basic frequencies of these systems probably have the same origin and are caused by similar physical mechanisms. Our results show that transient sources like XTE J1701-462, BHCs, and 4U 1608-52 are on the main track, while persistent sources, such as typical Z sources and 4U 1728-34, are shifted from the main track. The persistent and transient sources probably have a similar physical mechanism in producing the basic frequencies, but the difference between these two systems may cause the shifted track in WK/PBK schema.

### 4.2. The Role of Accretion Rate $\dot{m}$ and the LT Precession Model

For a given source, mass and spin do not change significantly, and most likely only the mass accretion rate ($\dot{m}$) determines $\nu_{\rm HBO}$ and $\nu_{\rm break}$. Extensive work has been done to study the spectral properties of GX 17+2 and XTE J1701-462 (Lin et al. 2009, 2012; Li et al. 2013). These authors suggested that the HBs of both GX 17+2 and XTE J1701-462 be interpreted by the same process acting at constant $\dot{m}$, namely an increase of Comptonization, while a changing $\dot{m}$ led to secular changes between subclasses. Table 3 shows that $\nu_{\rm HBO}$ and $\nu_{\rm break}$ increase along HB in both sources at a constant $\dot{m}$, which suggests that the values of $\nu_{\rm HBO}$ and $\nu_{\rm break}$ may be independent with $\dot{m}$, however, under the assumption of certain spectral models.

Several models have been proposed to study LFQPOs. Ingram et al. (2009) described a promising truncated disk/hot inner flow Lense–Thirring (vertical) model to interpret the characteristic frequencies seen in the broadband PSD of BH and NS. Within this model, the frequencies of LFQPOs are mostly dependent on the inner radius of the disk, while the break frequency is set by the viscous timescale at the outer edge of the flow (inner radius of disk). The ~1 Hz LFQPOs detected in dipping/eclipsing NS-LMXBs also suggested that LT procession models for LFQPOs are possible in NS-LMXBs (Homan 2012). The LT precession relation ($\nu \propto R^{-3}$) arose in GX 17+2, as introduced by Lin et al. (2012). However, Li et al. (2014) found that $\nu_{\rm HBO}$ in XTE J1701-462 is positively correlated with an inner disk radius based on using the same spectra model with GX 17+2, which makes the LT model an impossible explanation for the HBOs in XTE J1701-462. They further proposed that HBOs come from a corona. In Figure 3, we show that part of the data from XTE J1701-462 overlap with IGR J17480-2446 (green dot), which was assumed to be a inappropriate candidate for LT precession (Altamirano et al. 2012). This makes LT precession a controversial model for explaining the HBOs in XTE J1701-462 or even in other Z sources. In general, the physical mechanism in WK/PBK correlations cannot be well interpreted with any model thus far.

### 4.3. The Physical Implications of HBO and Break Components

Table 5 shows $\rm rms_{break}$ increasing linearly with energy below ~12 keV at a constant slope ($a = 0.200 \pm 0.004$) for XTE J1701-462 in both Cyg-like and Sco-like stages, while $\rm rms_{HBO}$ also shows the same trend with energy at a constant slope ($a = 0.100 \pm 0.001$). Both $\rm rms_{break}$ and $\rm rms_{HBO}$ stay stable when the energy is above ~12 keV, which is similar to what has been seen for the kHz QPOs (Berger & van der Klis 1996; Méndez et al. 2001). In addition, Figure 6 shows that both $\rm rms_{break}$ and $\rm rms_{HBO}$ decrease along HB, and Figure 7 also shows that these two components correlate with each other. These above results suggest that break and HBO components may come from a similar physical mechanism. Break and HBO signals reach the strongest strength at ~12 keV indicates that they come from higher energy photons, most likely from non-thermal emission from corona, since thermal emission from the disk could not produce such high energy photons. Li et al. (2014) also suggested that the HBO components in XTE J1701-462 are possibly generated from Comptonization emission in a corona, based on the spectral fitting results. Here, we further suggest that Comptonization emission in the corona contributes to both break and HBO components in XTE J1701-462. These two components could be caused by the same kind of oscillation in a corona with uneven density, and they could be produced in different areas of the corona. If break and HBO components come from different areas, they could differ in oscillation frequencies.

GX 17+2 and XTE J1701-462 are Z sources, and the spectral evolution in GX 17+2 was very similar to XTE J1701-462 in its Sco-like stage (Lin et al. 2012). Our results in Figure 6 also show that these two sources have similar variability properties in the Sco-like stage. Both $\rm rms_{HBO}$ and $\rm rms_{break}$ decrease with increased source intensity, with hardness decreasing at the same time. Their power spectra resemble each other and they have similar HBO frequencies. In particular, the variations of $\rm rms_{HBO}$ and $\rm rms_{break}$ in interval E (GX 17+2) are similar with that of interval D (Sco-like stage in XTE J1701-462). These evidences indicate that break and HBO components in GX 17+2 probably have a similar origin as in XTE J1701-462.

Figure 7(b) shows that $\rm rms_{HBO}$ has a power-law relation with $\rm rms_{break}$ for both sources. The data of GX 17+2 lay between the points of HB and the HB/NB vertex of XTE J1701-462. The spectral properties of GX 17+2 are found to be very similar to those of XTE J1701-462 in its Sco-like stage: the HB is associated with Comptonization of disk emission while at the HB/NB vertex the disk assumes a slim disk solution (Lin et al. 2012; Li et al. 2014). For XTE J1701-462, the different distribution between HB and the HB/NB vertex could be caused by the sudden reduction of Comptonization emission when approaching the HB/NB vertex. The connection of non-thermal emission and HBO was found in XTE J1701-462 and GX 17+2: the strength of Comptonization emission decreases when the HBO frequencies increase from upturn to HB, while the HBO signal disappears when Comptonization emission become undetectable on the NB. As shown in Figure 6, for XTE J1701-462, Cyg-like intervals generally have larger values of rms (break and HBO) than Sco-like intervals, while the range of rms of GX 17+2 is consistent with the Sco-like interval D of XTE J1701-462. We suggest this could be caused by different proportions of Comptonization component in total flux: the proportion of the Comptonization component in the Cyg-like stage is higher than in the Sco-like stage, which causes higher rms in the Cyg-like stage. The proportion of the Comptonization component in the Sco-like stage (GX 17+2) is higher than at the HB/NB vertex, which causes the lowest rms to take place at the HB/NB vertex. Thus, the three distinguishable tracks contributed by HB, GX 17+2, and the HB/NB vertex could

be caused by different proportions of Comptonization in the total flux.

### 4.4. The Accretion Disk Instability Model

The transient properties of some sources can be interpreted by the disk instability model (Lasota 2001), which assumes that the accretion disk gains mass from the mass donor at a constant mass transfer rate. The accretion rate is normally lower than the mass supply rate in the disk, thus mass is accumulated in the disk. When the accumulated mass exceeds a certain critical value, a sudden increase of accretion rate results in an outburst. By contrast, the persistent systems have a relatively stable accretion disk. The accretion disk tends to be more unstable in transient sources when they have an outburst, which would affect the oscillation in corona. This could be a reason why transient sources have a wider variation in $\nu_{\rm HBO}$ and $\nu_{\rm break}$ in WK/PBK schema if they are assumed to arise from different areas of corona. The persistent sources shifted from main track could be caused by the size of corona in persistent sources is different from transient sources. All of these suggestions still require further study.

## 5. SUMMARY

In this article, we studied the HBOs and band-limited components observed in the unique transient Z source XTE J1701-462 and the persistent "Sco-like" Z source GX 17+2. Our results show that the WK/PBK main track forms a boundary that separates persistent sources from transient sources. The shifted Z track is probably not caused by a misidentification of harmonics. The characteristic frequencies are independent of accretion rate in both GX 17+2 and XTE J1701-462, under the assumption of certain spectral models. We suggest that the HBO and break components from both sources probably come from a similar physical mechanism: Comptonization emission in the corona. These two components could be caused by the same type of oscillation in the corona with uneven density, and they could be produced in different areas of the corona. We suggest that it is the different proportions of the Comptonization component in total flux that cause the difference distribution between GX 17+2 and XTE J1701-462 in the $\rm rms_{break}$–$\rm rms_{HBO}$ diagram.

We are grateful to Y. N. Wang, H. Q. Gao, and Z. Zhang for data reduction and theory suggestions. This research has made use of data obtained from the High Energy Astrophysics Science Achieve Research Center (HEASARC) provided by the NASA Goddard Space Flight Center. This work is supported by the National Basic Research Program (973 Program) of China (grant No. 2014CB845800), the National Basic Research program (973 program) of China (grant No.2009CB824800), the National Natural Science Foundation of China (11173024), and the Fundamental Research Funds for the Central Universities, the Strategic Priority Research Program on Space Science, the Chinese Academy of Sciences, grant No. XDA04010300. T. M. Belloni acknowledges support from INAF PRIN 2012-6.

## REFERENCES

Altamirano, D., Ingram, A., van der Klis, M., et al. 2012, ApJL, 759, L20
Barret, D., & Vedrenne, G. 1995, ApJS, 92, 505
Barret, D., Olive, J. F., Boirin, L., et al. 2000, ApJ, 533, 329
Berger, M., van der Klis, M., van Paradijs, J., et al. 1996, ApJL, 469, L13
Berger, M., & van der Klis, M. 1998, A&A, 340, 143
Belloni, T., & Hasinger, G. 1990, A&A, 230, 103
Belloni, T., Psaltis, D., & van der Kils, M. 2002, ApJ, 572, 392
Belloni, T., Parolin, I., & Casella, P. 2004, A&A, 423, 969
Belloni, T., Homan, J., Casella, P., et al. 2005, A&A, 440, 207
Casella, P., Belloni, T., Homan, J., & Stella, L. 2004, A&A, 426, 587
Casella, P., Belloni, T., & Stella, L. 2005, ApJ, 629, 403
Cui, W., Zhang, SN., & Chen, W. 2000, ApJL, 526, L33
Dieters, S., & van der Klis, M. 2000, MNRAS, 311, 201
Done, C., Gierlinski, M., & Kubota, A. 2007, A&ARv, 15, 1
Hasinger, G., & van der Klis, M. 1989, A&A, 225, 79
Hasinger, G., van der Klis, M., Ebisawa, K., Dotani, T., & Mitsuda, K. 1990, A&A, 235, 131
Heindl, W. A., & Smith, D. M. 1998, ApJL, 505, L35
Homan, J., Wijnands, R., van der Klis, M., et al. 2001, ApJS, 132, 377
Homan, J., van der Klis, M., Jonker, P. G., et al. 2002, ApJ, 568, 878
Homan, J., & Belloni, T. 2005, Ap&SS, 300, 107
Homan, J., van der Klis, M., Fridriksson, J. K., et al. 2010, ApJ, 719, 201
Homan, J. 2012, ApJL, 760, L30
Ingram, A., Done, C., & Fragile, P. C. 2009, MNRAS, 397, L101
Jahoda, K., Markwardt, C. B., Radeva, Y., et al. 2006, ApJS, 163, 401
Lasota, J.-P. 2001, NewAR, 45, 449
Li, Z. S., Chen, L., Qu, J. L., et al. 2013, ApJ, 767, 167
Li, Z. S., Chen, L., Qu, J. L., et al. 2014, ApJ, 786, 119
Lin, D., Remillard, R. A., & Homan, J. 2009, ApJ, 696, 1257
Lin, D., Remillard, R. A., Homan, J., & Bareet, D. 2012, ApJ, 756, 34
Méndez, M., van der Klis, M., & Ford, E. C. 2001, ApJ, 561, 1016
Motta, S. E., Muñoz-Darias, T., Casella, P., Belloni, T. M., & Homan, J. 2011, MNRAS, 418, 2292
Nowak, M. A 2000, MNRAS, 318, 361
Olive, J. F., Barret, D., Boirin, L., et al. 1998, A&A, 333, 942
Psaltis, D., Belloni, T., & van der Klis, M. 1999, ApJ, 520, 262
Remillard, R. A., Sobczak, G. J., Muno, M. P., & McClintock, J. E. 2002, ApJ, 564, 962
Remillard, R. A., & Lin, D. 2006, Atel, 696
Rezzolla, L., Yoshida, S., Maccarone, T. J., et al. 2003, MNRAS, 344, L37
Sanna, A., Méndez, M., Altamirano, D., et al. 2010, MNRAS, 408, 622
Schnittman, J. D., Homan, J., & Miller, J. M. 2006, ApJ, 642, 420
Stella, L., & Vietri, M. 1998, ApJL, 492, L59
Tagger, M., & Pellat, R. 1999, A&A, 349, 1003
Titarchuk, L., & Osherovich, V. 1999, ApJL, 518, L95
van der Klis, M. 1989, in Timing Neutron Stars, ed. H. Ögelman & E. P. J. van der Heuvel (Dordrecht: Kluwer), 27
van der Klis, M. 1994a, A&A, 283, 469
van der Klis, M. 1994b, ApJS, 92, 511
van der Klis, M. 1995, in X-ray Binaries, ed. W. H. G. Lewin et al. (Cambridge: Cambridge Univ. Press), 252
van der Klis, M. 2006, in Compact Stellar X-ray Sources, ed. W. H. G. Lewin & M. van der Klis (Cambridge Astrophysics Series, Vol. 39; Cambridge: Cambridge Univ. Press), 55
Wagoner, R. V., Sirbergleit, A. S., & Ortega-Rodríguez, M. 2001, ApJL, 559, L25
Wijnands, R., Homan, J., & van der Klis, M. 1997, ApJL, 490, L157
Wijnands, R., & van der Klis, M. 1999a, ApJ, 514, 939
Wijnands, R., Homan, J., & van der Klis, M. 1999b, ApJL, 526, L33
Zhang, S. N. 2013, FrPhy, 8, 630